Title: **Emergence and evolution of the South Atlantic Anomaly revealed by the new paleomagnetic reconstruction SHAWQ2k**

S. A. Campuzano[1,2,†,*], M. Gómez-Paccard[2], F. J. Pavón-Carrasco[1,2], M. L. Osete[1,2]

[1]Dpto. de Física de la Tierra y Astrofísica, Universidad Complutense de Madrid (UCM), Avd. Complutense s/n, 28040-Madrid, Spain. E-mail: sacampuzano@ucm.es; fjpavon@ucm.es; mlosete@ucm.es.

[2]Instituto de Geociencias IGEO (UCM, CSIC), Calle Severo Ochoa 7, Edificio Entrepabellones 7 y 8, 28040-Madrid, Spain. E-mail: mgomezpaccard@csic.es.

[†]Now at: Istituto Nazionale di Geofisica e Vulcanologia (INGV), Via Vigna Murata, 605, 00143-Rome, Italy.

* Corresponding author: sacampuzano@ucm.es. Facultad de CC. Físicas. Universidad Complutense de Madrid. Avda. Complutense s/n. 28040 – Madrid (Spain).

Keywords: Geomagnetic Field Model, Quality paleomagnetic data, South Atlantic Anomaly

Abstract

The South Atlantic Anomaly (SAA) is one of the most outstanding features of the present geomagnetic field. Thus, a good knowledge of the SAA is clue for a better understanding of the dynamical behavior of the geomagnetic field. To achieve this goal, paleomagnetic data are crucial since they provide the unique way to investigate past changes in the Earth´s magnetic field. Here, we present a new global geomagnetic field reconstruction, the SHAWQ2k model, which is based on a critical revision of the global archeomagnetic and volcanic dataset. The new model provides an improved description of the geomagnetic field during the last 2 millennia, and yields surprising outcomes about the emergence and development of the SAA. It shows that the reversed flux patch observed at the core-mantle boundary and linked to the SAA, emerged in the Southern Hemisphere from at least 950 AD. This patch moved westward from the equator to southern latitudes, being clearly isolated after 1400 AD. In addition, since 1550 AD a second reversed flux patch moving northeastward is observed in the North Atlantic. The new data now available for the Southern Hemisphere coming from Africa and South America together with the use of an appropriated weighting scheme in the modeling process have improved our understanding of past geomagnetic field behavior and showed new evolutionary aspects of the SAA.

1. Introduction

Since 1840, when direct measurements of the geomagnetic field intensity became available, the dipole moment has experienced a decrease of 9% (from 85 to 78 Z Am^2). This decaying trend has been accelerated since 1990 [Thébault et al., 2015]. The modern decay of the dipole moment is contemporaneous to the emergence on Earth's surface of an area of low field intensity spanning the southern Atlantic Ocean, Africa and South America, known as the South Atlantic Anomaly (SAA). The SAA is one of the most intriguing features of the present geomagnetic field [Hulot et al., 2002; Olson & Amit, 2006; Aubert, 2015]. The presence of the SAA, which causes field asymmetry, has in fact been recognized as an essential ingredient to explain the decreasing trend of dipole intensity [e.g., Finlay et al., 2016]. Some authors do even propose that the present expansion of the SAA can be interpreted as an indicator of an impending reversal of Earth's magnetic field [e.g. De Santis et al., 2013; Laj & Kissel, 2015]. The link between geomagnetic field anomalies at Earth´s surface and reversed magnetic flux patches (RFP) at the core-mantle boundary (CMB) has been widely discussed in the literature. For example, Hulot et al. [2002] associated the growth of the South African reversed patch at the CMB with the present decrease of the dipole field and the SAA at the Earth´s surface. Gubbins et al. [2006] proposed that this RFP emerged in the Southern Hemisphere around 1840 AD. However, Suttie et al. [2011] suggested an earlier onset of the dipole decay, in the seventeenth century. More recently, Tarduno et al. [2015] pointed that the SAA could be responsible of the low paleointensities observed in Southern Africa around 1300 AD. They also suggested that the unusual CMB composition and structure beneath Southern Africa (associated with a low seismic wave anomaly in the lowermost mantle) promote core flux expulsions resulting in low field strengths at the Earth's surface. In addition, they postulated that this region might have been a steady site for flux expulsion, and hence for triggering geomagnetic field reversals, for millions of years. This hypothesis is also supported by Shah et al. [2016] who found evidence of a low intensity anomaly in the South Atlantic region, similar to the recent SAA, during the Late Pleistocene.

The proposed past behavior of the SAA is obtained from paleomagnetic data or geomagnetic field reconstructions based on them. However, two problems have to be addressed for this purpose: the spatial and temporal scarcity of paleomagnetic data and their apparent variable accuracy.

Fortunately, during the last decade, a considerable effort has been made to obtain new data from unexplored regions such as the Southern Hemisphere, a key point to better constrain the evolution of the SAA. Crucial data have been obtained for Africa [Neukirch et al., 2012; Mitra et al., 2013; Donadini et al., 2015; Tarduno et al., 2015; Osete et al., 2015; Kapper et al., 2017] and South America [Goguitchaichvili et al., 2012, 2015; Roperch et al., 2014, 2015; Poletti et al., 2016]. These recent paleointensity data have, in general, been obtained applying minimum standards of quality that were not common a few decades ago [e.g. Genevey et al., 2008; Paterson et al., 2014; Cromwell et al., 2015]. It has been recognized that some of the older studies may contain some paleointensities that might not be accurate markers of the past geomagnetic field [e.g. Chauvin et al., 2000, Genevey et al., 2008; Paterson et al., 2014]. Despite this situation, global geomagnetic field models are commonly constructed without consideration of the different accuracy of the data used [e.g. Constable et al., 2016; Licht et al., 2013; Nilsson et al., 2014; Pavón-Carrasco et al., 2014a]. Here, we follow a new approach by implementing a global geomagnetic field model for the last 2 ka based, for the first time, on a weighting scheme of the global paleomagnetic dataset which takes into account all these quality standards especially relevant in paleointensity studies. The new model, the SHAWQ2k, enables discussing the past geomagnetic field with unprecedented resolution, and provides a better understanding of the SAA evolution.

2. Methods

Our initial hypothesis is that at the present stage, the high scatter of the global paleomagnetic dataset, mostly related to potentially low-quality paleointensities, is hampering a proper monitoring of the major characteristics of the geomagnetic field, and in particular of the SAA. Here we propose a new approach to consider the accuracy of paleomagnetic data during the modeling process. This approach consists on giving higher weights to the paleomagnetic data that we deem the most accurate. In order to avoid the documented problems associated to sedimentary sequences such as the smoothing effect , the compaction-induced inclination errors [e.g. Tarduno et al., 1990; Tauxe, 1993; Roberts et al., 2013 and references therein] or magnetic mineral diagenesis [e.g. Tarduno et al., 1998, and references therein], we only use paleomagnetic data derived either from archeological remains

(e.g. kilns, hearths, pottery…) or from volcanic units, which acquired their magnetization through a thermoremanence (TRM) mechanism, which is firmly linked with the Néel's theory [Néel, 1955]. If the age of the last heating-cooling cycle affecting the archeological material or rock is known, these data provide spot records of the ancient geomagnetic field. In addition, we decided to restrict our study to the last 2 ka (from 100 BC to 1900 AD) since the majority of archeomagnetic and volcanic data (more than 90%) correspond to this time interval [Brown et al., 2015].

To compile the raw database we used the global compilations ArcheoInt, [Genevey et al., 2008] and GEOMAGI50v3.2 [Brown et al., 2015] updated with the most recent studies published up to December 2017 and not contained in the aforementioned databases (see Section 1 of the Supplementary Material). These new publications are especially important since they provide data from very poorly covered areas, such as Africa and South America. We label as AV (Archeo-Volcanic) this database, which includes 3085 declinations, 4355 inclinations and 2259 intensities (see Table 1Sa). Once compiled, we ranked the AV data into two different categories following different quality criteria based on the type of material analyzed, the number of specimens used, and the laboratory protocol followed to obtain the final value presented in the databases [see e.g. Pavón-Carrasco et al., 2014b]. First, we consider the number of specimens involved in the calculation of both the directional and intensity means. This is undoubtedly a crucial point to determine if a mean value is sufficiently accurate. The more specimens or samples we use, the greater the statistical confidence on the mean value, although one should also be mindful that this precision does not always correspond to higher accuracy. Beyond n=3, which can be justified as a minimum on the basis of Fisherian statistics, the choice of a minimum number of samples/specimens is somewhat subjective. In this study we decided to use a minimum of 4 specimens to consider a mean direction or intensity as a high-quality data (here-and-after denoted as Q-data). When the number of specimens is not available, we consider that they were obtained from 1 specimen (when no error is given associated to the mean) or 2 (if an error is provided). Therefore these data were automatically classified as low quality. Second, we consider the experimental protocol applied for paleointensity determination since we consider that this is a key point for obtaining accurate intensity measurements. It is generally accepted that the most efficient intensity protocols are those based on -or derived from- the Thellier type technique [Thellier

139 & Thellier, 1959]. Moreover, modern standard of quality includes the evaluation (via the so-called
140 pTRM checks) of potential magnetochemical changes induced during the laboratory intensity
141 protocol, as well as the quantification of the TRM anisotropy effect upon paleointensity values that
142 can be experimentally estimated via the determination of anisotropy ellipsoids [e.g. Chauvin et al.,
143 2000; Genevey et al., 2008; Paterson et al., 2014]. We hence consider that Q-data correspond to
144 intensity values derived from experiments based on the Thellier-Thellier type methods, including
145 pTRM checks and for which the TRM anisotropy correction has been considered if they were
146 obtained from potentially highly anisotropic archeological objects (such as pottery or ceramics). Since
147 the effect of the TRM anisotropy in volcanic samples is usually low, the TRM anisotropy correction
148 is not required for this kind of samples. These Q-data constitute that we have called the QAV (Quality
149 Archeo-Volcanic) dataset, which includes 2858 declinations, 3062 inclinations and 442 intensities (see
150 Table 1Sb).

151 The spatial and time distributions of the AV and QAV databases are represented in Fig. 1.
152 As expected, the intensity is the parameter most affected by the quality selection criteria applied,
153 being only 20% of the intensities included in the Q-data, whereas the 93% of declinations and the
154 70% of inclinations are included. Q-data are clearly concentrated in the Northern Hemisphere (98%
155 of them, Fig. 1, left panels), but the recent incorporation of intensities from Africa and South America
156 greatly improves the spatial coverage in the Southern Hemisphere. However, the number of Q-data
157 in this area is still rather low. Directional data are also very scarce for South America with only one
158 available archeomagnetic datum from Bolivia [Eighmy, 2003], and 7 volcanic data from Chile
159 [Roperch et al., 2014, 2015]. The time distribution panel (Fig. 1, right side) shows an approximately
160 homogeneous distribution for the last two millennia. A decrease in the number of declination and
161 inclination data is observed around 500 AD, probably due to the scarcity of well-preserved *in situ*
162 archeological remains for this period. The sharp decrease in the number of Q-inclination data for the
163 last 500 years (1400 – 1900 AD) is mainly due to data from Eastern Europe and Russia [Burlatskaya
164 et al., 1986] for which the number of specimens used is not given in the corresponding articles and
165 hence were not included in QAV dataset.
166

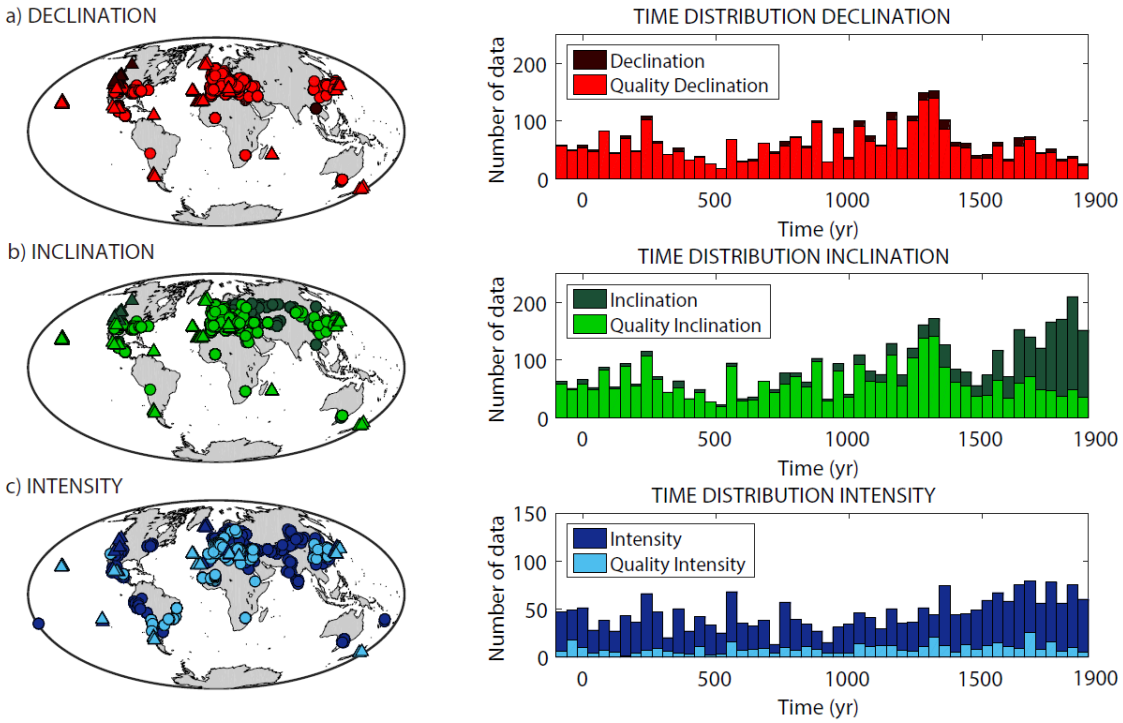

167

168 **Fig.1. Data distribution.** Spatial and temporal distribution of (a) declination, (b) inclination and (c)
169 intensity data derived from the paleomagnetic study of baked archeological materials (circles) and
170 volcanic samples (triangles) corresponding to the last 2 ka (100 BC – 1900 AD). Light colours
171 correspond to Q-data (QAV database) and dark colours to the complete database (AV database).

172

173 Then two additional filters (Filters 1 and 2 in Table 1Sa-b) were applied (following e.g. Korte
174 et al., 2009). We rejected paleomagnetic estimations corresponding to errors higher than 3 times the
175 mean of the angle α_{95} (related to declination and inclination uncertainties) or 3 times the mean of the
176 standard deviation of the intensity values. Data associated with age uncertainties higher than 250
177 years were also discarded. After filtering, the AV dataset includes 2928 declinations, 4141 inclinations
178 and 2160 intensities (see Table 1Sa) and the QAV dataset includes 2694 declinations, 2898
179 inclinations and 435 intensities (see Table 1Sb).

180 Korte et al. [2009] noted that the application of strict selection criteria produces a strong
181 reduction of the number of data, preventing the implementation of reliable geomagnetic field models.
182 For this reason, the first issue that should be addressed is if a robust reconstruction of the past
183 geomagnetic field can be derived using only the compiled QAV database. For testing this point, we
184 have performed some studies and two synthetic tests using the IGRF-12 [Thébault et al., 2015] and

SHA.DIF.14k [Pavón-Carrasco et al., 2014a] models that are described in detail in the Supplementary Material (section 2, Fig. 1S-4S and Table 2S). These tests suggest that there is currently not enough Q-data to obtain a robust global geomagnetic field model for the last 2 ka. Consequently, additional data are needed to better constrain the inversion process. To solve this problem, we propose here a novel approach that allows considering the complete AV database (i.e. also data not included in the Q-data category) by using an appropriated weighting scheme based on data quality. To do that, the most difficult problem is to establish the relative ratio between the weight assigned to the data that we deem the most accurate (w_Q corresponding to Q-data) and the weight (w) corresponding to the other paleomagnetic estimations. To quantify the w_Q/w ratio we constructed different geomagnetic field models using different ratios (from 1 to 100). From these models, we synthesized declination, inclination and intensity data at the same locations than those corresponding to the Q-data in the original database. We then compared the predictions of the model obtained with real Q-data by calculating the normalised root mean square (n-rms) error. Fig. 5S of the Supplementary Material shows that for different damping parameters the trade-off curves of n-rms and weighting ratios present a knee point around 10 ($w_Q/w = 10$), showing the best compromise between the modeling fitting and the proposed weighting scheme. For the particular case where $w_Q/w = 1$, i.e. the data are not weighed during the modeling process, we provide the coefficients of the resultant geomagnetic reconstruction called as SHA.AV.2k (see section 2 in Supplementary Material for more details) in the Table 3S of the Supplementary Material.

For modeling purposes, we followed the same approach as the work of Korte & Constable [2005] i.e. the Spherical Harmonic Analysis (SHA) technique in space and the penalized cubic B-splines [De Boor, 2001] in time. We selected the maximum degree of the harmonic expansion equal to 10 and we fixed the temporal knot points every 25 years between 200 BC and 2000 AD (we add 100 yr at the beginning and end of the original time interval to avoid edge effects). The residuals (differences between the real and modelled data) are used for identifying and rejecting outliers following the classical approach used by the paleomagnetic modeling community. For this purpose, we performed a first guess model and data corresponding to residuals greater than 3 times their standard deviation were rejected (see Filters 3 and 4 in Table 1S). This supposes the rejection of 8.1%

213 of the AV database (see Table 1S). Finally, in order to estimate model uncertainties, a bootstrap
214 technique (similar to that described in Korte & Constable, 2008) was applied. A set of *M* models were
215 generated by slightly perturbing the input data with two random distributions: 1) a Gaussian
216 distribution centred in the mean directional and intensity values with a standard deviation given by
217 the corresponding errors; and 2) an homogeneous distribution centred in the mean age of the data
218 with an amplitude equal to their uncertainty. The inversion was regularized at the core-mantle
219 boundary by means of the damping parameters α and τ between 10^{-9} and 10^{-8} μT^{-2} for space and
220 between 10^{-5} and 10^{-4} $\mu T^{-2}yr^{4}$ for time, respectively (see the Supplementary Material for more
221 information). These damping parameters were obtained following Pavón-Carrasco et al. [2014a] and
222 Licht et al. [2013].
223
224 ## 3. Results
225 ### 3.1. A new reconstruction of the geomagnetic field: the SHAWQ2k global model
226 The first global geomagnetic field reconstruction that uses a weighting scheme based on
227 paleomagnetic data qualities (according to the criteria used) is presented here: the SHAWQ2k model.
228 "SHA" indicates the mathematical modeling technique used (Spherical Harmonic Analyses); "WQ"
229 highlights that the model is computed considering a weighting scheme related to a quality ranking of
230 the input data (the complete AV database filtered by Filters 1-4 in Table 1Sa); and finally "2k" refers
231 to the time interval covered by the model (100 BC - 1900 AD).
232 The final number of data used to compute the SHAWQ2k model after rejection outliers
233 (Table 1S, filters 2-3) is 2813 declinations, 3986 inclinations and 2111 paleointensities. The values of
234 the α and τ parameters involved in the spatial and temporal regularization at the core-mantle
235 boundary (CMB) are set to $10^{-8}\mu T^{-2}$ and $10^{-4}\mu T^{-2}yr^{-4}$, respectively (Fig. 6S). No additional
236 regularizations were applied, i.e. we do not impose a convergence with the historical models available
237 for the last centuries.
238 A total of 6 iterations were needed to obtain the final set of Gauss coefficients (120 time-
239 dependent coefficients as it corresponds to degree 10). The Gauss coefficients' uncertainties were
240 obtained by a bootstrap approach using a set of 5000 models (M=5000). Both the Gauss coefficients

241 and the associated uncertainties at 1-σ are given in Table 4S. The final n-rms misfits obtained were
242 1.0 for declination, 1.5 for inclination and 1.4 for intensity, being 1.3 the overall value. For a more
243 detailed discussion on the n-rms errors see section 3 of the Supplementary Material (Fig. 7S).

244 The different harmonic contribution of the SHAWQ2k Gauss coefficients can be analysed
245 using the power spectra and its secular variation. The time-average results are shown in Fig. 8S
246 together with their uncertainties. Results are compared with other published paleomagnetic and
247 instrumental global models. Both the power spectra and its secular variation are similar for all the
248 paleomagnetic models considered up to degree 6. The model IGRF-12 also agrees with the
249 SHAWQ2k model up to degree 6 for the power spectra and up to degree 4 for the secular variation.

250 The ability of the SHAWQ2k model to reconstruct local scale geomagnetic field variations
251 has been also evaluated by comparing the local paleosecular variation curves (PSVC) predicted by the
252 model with the input data available for 6 different regions corresponding to different data densities.
253 In Europe, we choose Paris (48.9ºN, 2.3ºE) to represent Western Europe and Sofia (42.7ºN, 23.3ºE)
254 to represent Eastern Europe. Asia is represented by the city of Shanghai (31.2ºN, 121.5ºE) and North
255 America by Boulder (40.0ºN, 105.3ºW). Honolulu (21.3ºN, 157.8ºW) has been chosen to represent
256 the central Pacific region, the area with more available volcanic data. The Southern Hemisphere is
257 represented by Rio de Janeiro (22.9ºS, 43.2ºW) in Brazil, where new data have been recently published
258 [Poletti et al., 2016]. The predicted PSVCs together with the input data located inside a region of 900
259 km of radio centered at the selected locations are plotted in Fig. 2. The data have been relocated to
260 the reference location following the virtual geomagnetic pole method [Noël & Batt, 1990]. Q-data
261 are represented in green and the rest of data (also used to obtain the model) in gray. Additionally, the
262 predictions of the global geomagnetic field models CALS3k.4 [Korte & Constable, 2011], ARCH3k.1
263 [Korte et al., 2009], pfm9k.1a [Nilsson et al., 2014] and SHA.DIF.14k are also shown.

264 In general, the SHAWQ2k results agree with the models based on archeomagnetic and
265 volcanic data (SHA.DIF.14k and ARCH3k.1). The main differences can be explained either by the
266 incorporation of new data (e.g. in Shanghai, Cai et al., 2014, 2016, 2017), or by the new weighting
267 scheme applied here and that allows considering data quality during the modeling process (e.g. in
268 Honolulu).

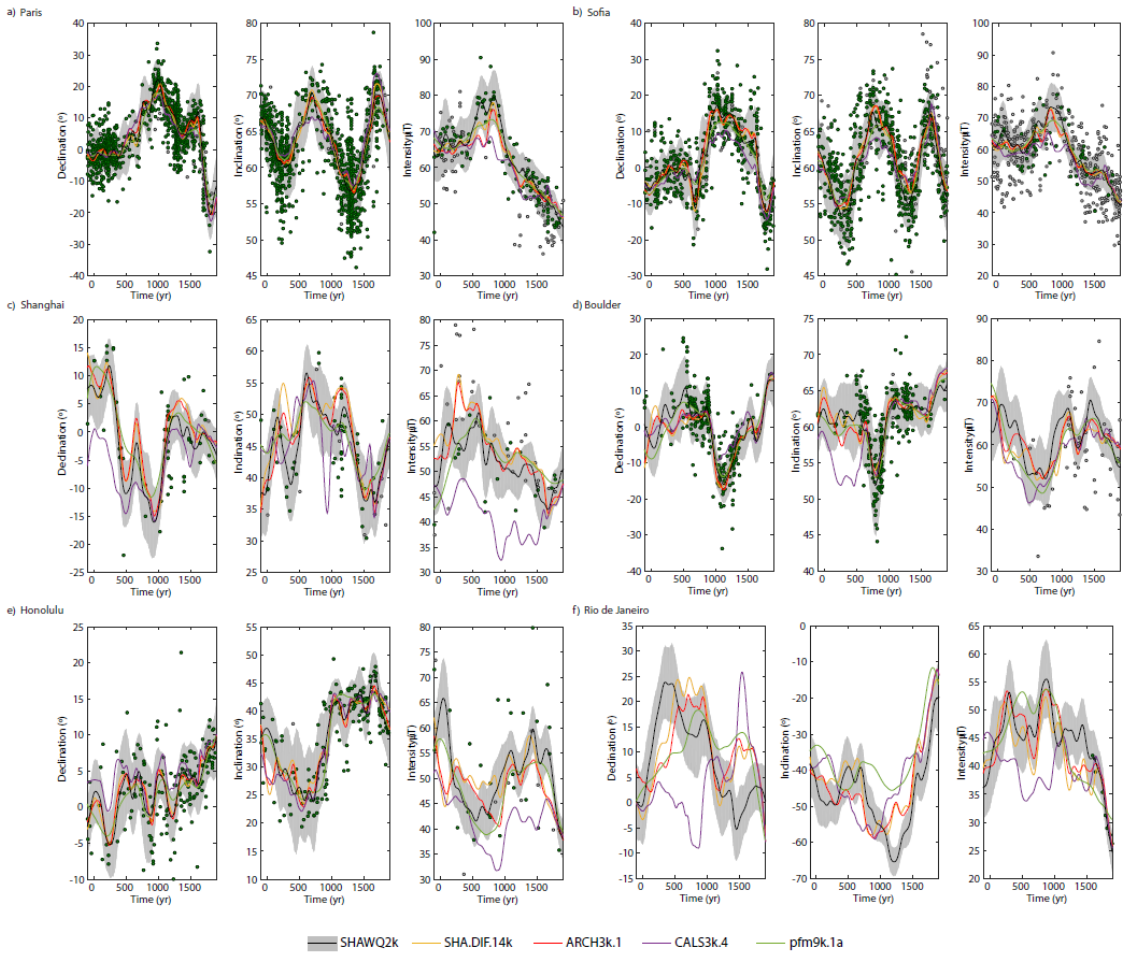

Fig. 2. Comparison between SHAWQ2k model predictions (black line and shaded gray area) and the input data (green circles for the Q-data and gray circles for the other data) at six selected locations a) Paris (France), b) Sofia (Bulgaria), c) Shanghai (China), d) Boulder (USA), e) Honolulu (Hawaii), f) Rio de Janeiro (Brazil). Declination, inclination and intensity values are represented together with their error band at level 95% of confidence for the SHAWQ2k model (black lines and shaded gray areas). For comparison, the SHA.DIF.14k (yellow line), ARCH3k.1 (red line), CALS3k.4 (purple line) and pfm9k.1a (green line) predictions are also plotted.

3.2. Dipole moment evolution over the last 2 ka

The dipole moment (DM) obtained from the SHAWQ2k model is shown in Fig. 3a. According to SHAWQ2k, the DM has experienced a stepwise decay over the last 2 ka, from a maximum value of ≈ 108 Z Am² reached around 80 AD to a minimum of ≈ 82 Z Am² observed at

283 the end of the temporal window considered (i.e. 1900 AD). This DM decrease corresponds to an
284 average rate of 0.007 Z Am^2/yr for the last 2 ka. Three maxima are observed at 80 AD, 890 AD (104
285 Z Am^2) and 1430 AD (96 Z Am^2). A consistent rate of DM decrease after these three maxima is
286 observed (of about 0.04-0.03 Z Am^2/yr). This value is similar to the DM decay rate observed between
287 1840 and 1900 AD (0.04 Z Am^2/yr, estimated from the GUFM1 model; Jackson et al., 2000). In
288 contrast, it is slightly higher from 1900 to 2015 AD, period that corresponds to a decay rate of 0.05
289 Z Am^2/yr (given by IGRF-12 model). The new DM reconstruction is compared with previous
290 models based on archeomagnetic and volcanic data (SHA.DIF.14k; ARCH3k.1) and on archeo,
291 volcanic and sedimentary data (CALS3k.4; CALS10k.2, Constable et al., 2016; and pfm9k.1a). Similar
292 that for PSVC regional variations, the main differences can be explained by the incorporation of
293 recent data in the SHAWQ2k model and/or by the implementation of the weighting scheme. We
294 then used the model SHAWQ2k to infer the position of both the north geomagnetic (or dipole, n =
295 1) and magnetic (n = 1 – 10) poles (Fig. 3b). A low tilt of the dipole and magnetic poles is observed
296 at the beginning of the time interval (100 BC-100 AD). Then, a subsequent sharp increase of the tilt
297 towards the Atlantic region (with angular displacements up to 8.2º for the geomagnetic and 20.3°
298 for the magnetic poles) can be seen up to 500 AD with a mean speed of 3.9 and 6.1 km/yr for the
299 geomagnetic and magnetic poles, respectively. Next, both poles drifted eastward. The geomagnetic
300 pole moves eastward since 500 AD and reaches the longitude of 115ºE at 1200 AD, with a mean
301 drift speed of 4.7 km/yr. From 1200 AD up to 1800 AD, the geomagnetic pole undergoes a rapid
302 drift (at a mean speed of 4.6 km/yr) from the eastern hemisphere towards the western following a
303 meridional trend, reaching 64.7°W at 1800 AD. On the other hand, the magnetic pole also moves
304 towards the western hemisphere with a mean drift speed of 5.7 km/yr from 1000 AD to 1800 AD,
305 when it reaches 115.6°W. It is important to notice that cusps in the geomagnetic pole appear to be
306 related with minima in dipole intensity (see Fig. 3b-c and Movie 1S in the Supplementary Material).
307 It seems that dipolar impulses cause changes of geomagnetic pole sense drift. The movement trend
308 of both poles was similar until 1800 AD, but being the movement of the north magnetic pole of
309 wider amplitude and higher speed than the geomagnetic pole movement. This behavior has also been
310 observed before by Korte & Mandea [2008] using the CALS7k.2 model [Korte & Constable, 2005].

311 For the last century (1800 - 1900 AD), the north geomagnetic pole remained located at western
312 longitudes. In contrast, during this interval the north magnetic pole experienced a rapid drift to the
313 eastern hemisphere with a mean speed of 12.7 km/yr. The tilt of the geomagnetic pole registers
314 maxima values of 11.2° around 925 AD, similar to those observed nowadays. This has also been
315 observed by Nilsson et al. [2010, 2011] which studied the dipole moment evolution using sedimentary
316 records distributed around the world including the Southern Hemisphere. On the contrary, using the
317 CALS7k.2 model, tilt values higher than 10° are not reached until 1800 AD [Korte & Mandea, 2008].
318 In terms of geomagnetic field energies (Fig. 3c), we observe a general decreasing trend for both the
319 dipole and non-dipole energies up to around 1750 AD. After this time, the non-dipole energy
320 increases while the dipole energy continues to decrease.

321

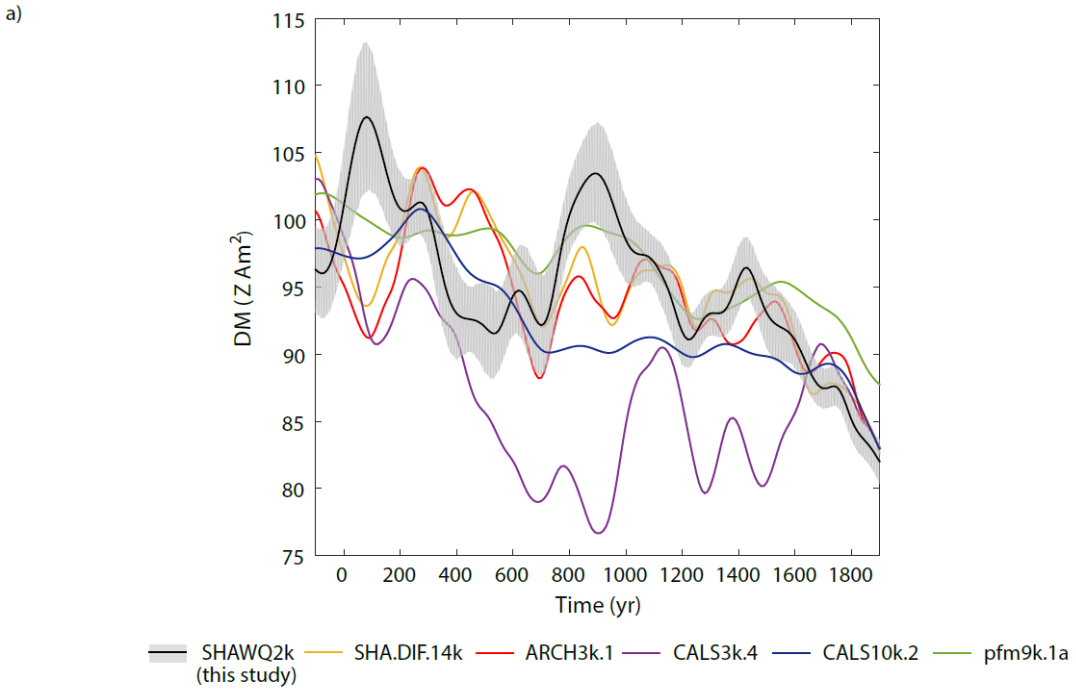
a)
DM (Z Am^2)
Time (yr)
SHAWQ2k (this study)
SHA.DIF.14k
ARCH3k.1
CALS3k.4
CALS10k.2
pfm9k.1a

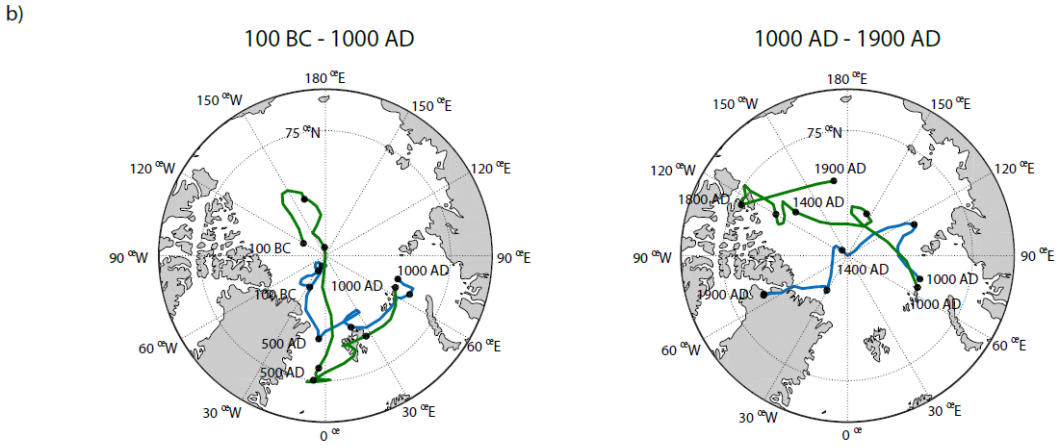
b)
100 BC - 1000 AD
1000 AD - 1900 AD
100 BC
1000 AD
500 AD
1400 AD
1900 AD

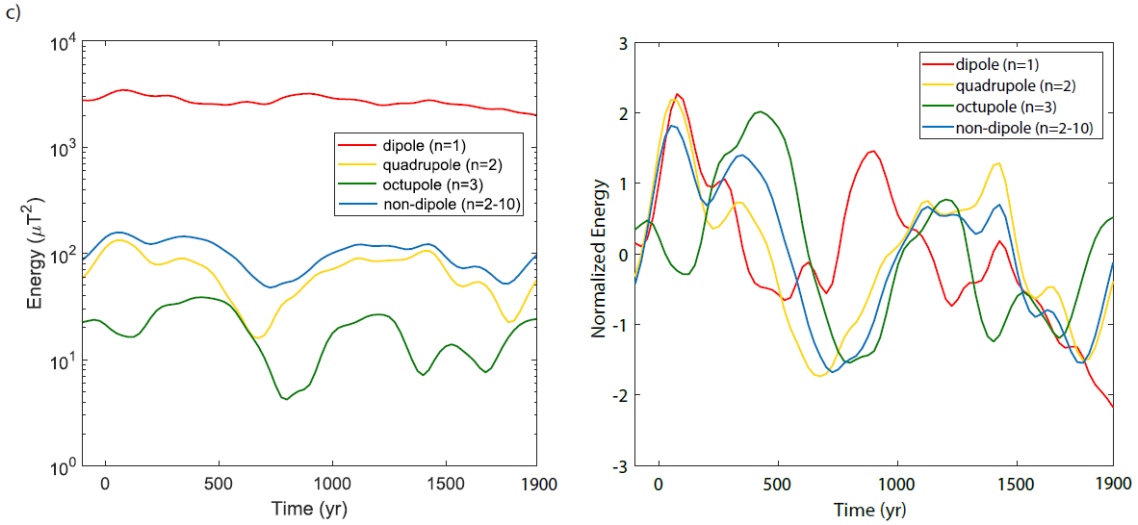
c)
Energy (μT^2)
Time (yr)
dipole (n=1)
quadrupole (n=2)
octupole (n=3)
non-dipole (n=2-10)
Normalized Energy

322

Fig. 3. Dipole moment reconstruction, north polar wander path over the last 2 millennia and harmonics contributions. a) Dipole moment reconstruction (black line) obtained from the new model SHAWQ2k along with the error band corresponding to one standard deviation (gray shaded area). The results are compared with previous global geomagnetic field models: SHA.DIF.14k (yellow line), ARCH3k.1 (red line), CALS3k.4 (purple line), CALS10k.2 (blue line) and pfm9k.1a (green line). b) Position of the north magnetic pole (green) and north geomagnetic pole (blue) for two different time periods: 100 BC to 1000 AD and from 1000 AD to 1900 AD. c) Energy evolution of the dipolar (red line), quadrupole (yellow line), octupole (green line) and non-dipolar (blue line) terms of the SHAWQ2k model at the Earth's surface. In the right panel, the normalized energy (mean zero and standard deviation one) is shown for facilitating the comparison.

3.3. Evolution of the geomagnetic field at the Earth's surface and at the core-mantle boundary over the last 2 ka

We have represented the geomagnetic field elements (i.e. declination, inclination and intensity) at the Earth's surface derived from the SHAWQ2k reconstruction. Maps every 500 yr are plotted in Fig. 4. The temporal continuous evolution of these elements can be found in Movie 2S of the Supplementary Material. This shows that a region of low equatorial intensities located in the Indian Ocean is clearly observed around 0 AD, but it is worth mentioning that probably this anomaly was already present in 100 BC (see Movie 2S for details). Then, this feature grew up and moved quickly towards the African continent, where it remained located for about 500 years showing the minimum value of intensity at 400 AD. This intensity minimum faded gradually and moved slightly eastward during the time interval 600-900 AD, coinciding with an eastern drift of the north geomagnetic and magnetic poles (Fig. 3b). Then, the anomaly grew up (up to 1200 AD) and moved quickly towards western longitudes, being located in South Africa around 1350 AD. It remained on this region up to 1700 AD, when moved westward and grew up in extent until its present configuration, which is known as the SAA.

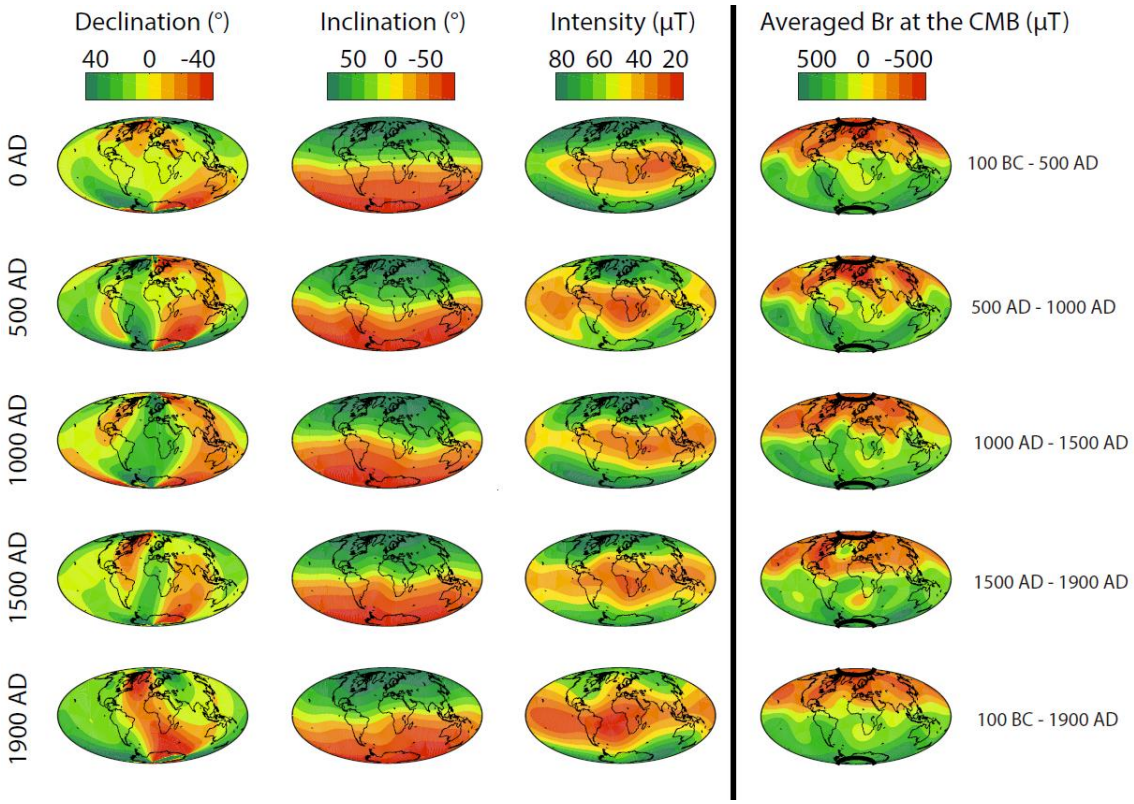

Fig. 4. Evolution of the geomagnetic elements at the Earth's surface together with the radial field at the CMB. Snapshots of declination, inclination and intensity obtained from the SHAWQ2k reconstruction and plotted every 500 yr (three first columns). The mean radial field (Br) at the CMB averaged every 500 yr using 500 yr window widths (last column) is also shown. Note that the last average plotted corresponds to the whole studied period (100 BC-1900 AD). The black circles in the last column indicate the projection of the tangent cylinder at surface.

The geomagnetic field variations observed at the Earth´s surface can be linked to the time-averaged radial field (Br) at the CMB. Fig. 4 (right column) provides 500-yr time-averaged Br maps at the CMB. In order to avoid shorter wavelengths contributions in Br estimations coming from higher degrees, we have used a maximum degree of the spherical harmonics equal to 6. The time-averages have been calculated to exclusively highlight long persistent flux lobes. These results reveal a reversed flux patch (RFP) located beneath the Southeast of the Arabic Peninsula at 1000 AD. This RFP was probably already present at 950 AD (see Movie 3S in the Supplementary Material for more details, where snapshots of Br every 50 years are showed). After 1000 AD, the RFP quickly moved southward and westward and was completely isolated around 1700 AD beneath South Africa. The

366 RFP continued growing in intensity until ≈1750 AD, when it sharply migrated westward and finally
367 reached the South Atlantic Ocean, where it is located nowadays.

368 The Br averages corresponding to 100 BC-1900 AD can be used to analyze the persistence
369 of the geomagnetic field features over the last 2 ka. Results at the CMB (Fig. 4) indicate that in the
370 northern hemisphere, three large areas of high normal flux are found and located underneath
371 Northern America, Northern Europe and Northeast Asia. This agrees with the results obtained by
372 Korte & Holme [2010] who suggest the persistence of these three normal flux patches (NFPs) at
373 high latitudes over the Holocene. In contrast, the present field as well as historical field averages only
374 show two NFPs at high latitudes in the northern hemisphere, being absent the lobe observed under
375 Europe (see e.g. Terra-Nova et al., 2017). These high latitude NFPs (within the region delimited by
376 the tangent cylinder) contribute to the dipolar configuration of the Earth's magnetic field (see e.g.
377 Hollerbach & Gubbins, 2007). In the Southern Hemisphere, only one persistent NFP, located at high
378 latitudes and covering half of the Antarctica continent projection at the CMB, is observed from our
379 new SHAWQ2k reconstruction. It is also worth noting the persistence of a NFP at mid-latitude
380 (beneath the Hawaiian sector) and a persistent RFP, located under Southern Africa and surrounding
381 areas. Interestingly, this area is roughly similar to the present day SAA area.
382

383 ## 4. Discussion: The emergence and evolution of the South Atlantic
384 ## Anomaly.

385 The SHAWQ2k reconstruction indicates a low-intensity anomaly located on African-Indian
386 longitudes at the beginning of the Common Era (Fig. 4 and Movie 2S). This anomaly has been
387 changing in extent and drifting until acquiring its present configuration, which is known as the SAA.
388 The mean average growing rate of this anomaly from 1000 AD to 1100 AD (estimated from the area
389 inside the intensity isoline of 33 μT, i.e. the expected value for those magnetic latitudes) was $1.6 \cdot 10^5$
390 km^2/yr, being quasi-stationary on the African-Indonesia hemisphere. From 1200 to 1400 AD the
391 anomaly experienced a westward drift until being located at African longitudes. Since 1400 AD, the
392 anomaly followed a westward drift and has been growing in extent with a mean rate of $1.9 \cdot 10^5$ km^2/yr.

At the CMB (Movie 3S), the SHAWQ2k model allows us to obtain an improved description of the spatial and temporal evolution of the RFP that was identified by Gubbins et al. [2006] as the responsible of the SAA. The SHAWQ2k model suggests that this RFP would have emerged much earlier than suggested by this pioneering work, i.e. around 1840 AD. According to our new model, the RFP was present since at least 950 AD. It is important to note that an improved description of this RFP is now available thanks to the new intensity data coming from Southern Africa [Tarduno et al., 2015]. Previous archeomagnetic and paleomagnetic reconstructions did not include these new data, and probably this explains the fact that Terra-Nova et al. [2015] did not observe any RFPs during the period 550–1440 AD. In order to deeply study the time of emergence of this RFP (named S-RFP in Fig. 5), we analysed in detail its evolution at the CMB from 1000 to 1900 AD according to the SHAWQ2k model.

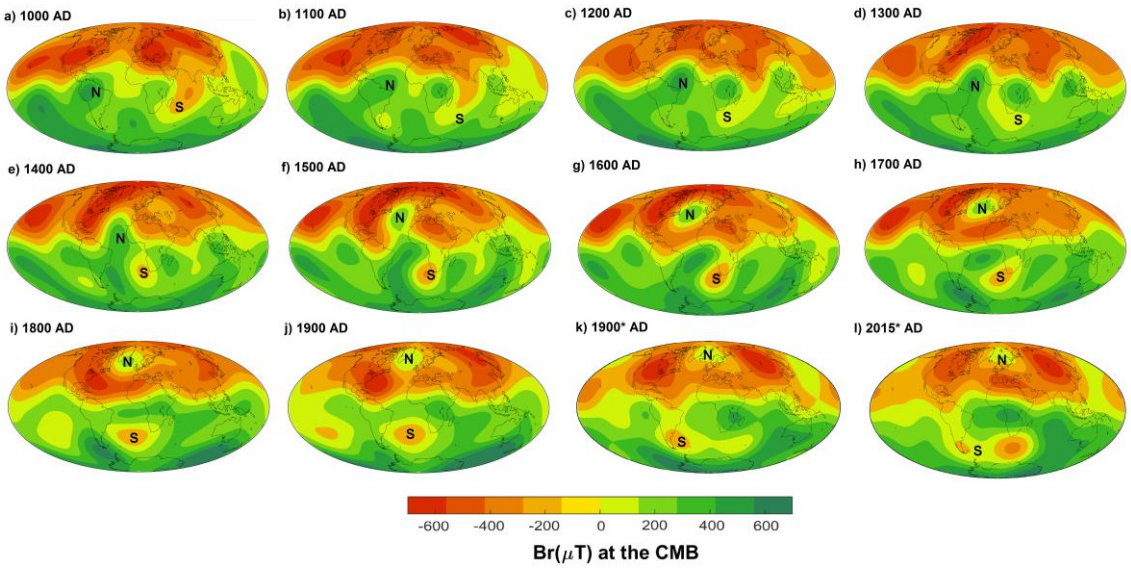

Fig. 5. Evolution of radial field at the CMB. (a-j) Radial field (Br) at the CMB computed for the last 1000 years every 100 years using the SHAWQ2k model. (k-l) Br maps calculated using the instrumental model IGRF-12 in 1900 and 2015 AD.

The snapshot maps of Br show that an area of reversed polarity located beneath the South of India penetrated from the magnetic equator and moved away southwest at a rate of 10.4 km/yr (0.2°/yr) from 1000 AD up to 1200 AD. This behaviour is constrained by 31 data (3 Q-data, coming from Syria, Genevey et al., 2003; and South Africa, Tarduno et al., 2015), which represents 3% of the

413 complete used database for this time interval. The S-RFP increased from -163.5 μT to -289.8 μT until
414 1550 AD (minima values corresponding to this lobe). In 1700 AD, it was isolated beneath South
415 Africa and started to shift westwards at a rate of 11.4 km/yr, until reaching the South Atlantic Ocean
416 in 1900 AD. In this year, the maximum intensity of the S-RFP was -203.0 μT, comparable to the
417 intensity of the S-RFP derived from the IGRF-12 model (-168.8 μT). Considering that the
418 SHAWQ2k reconstruction does not include historical data neither regularization based on historical
419 models at the end of the temporal windows, the noticeable agreement observed for 1900 AD makes
420 us be confident on our model, in spite of the significant scarcity of the paleomagnetic database used.
421 We have also plotted the Br map at the CMB for 2015 according to the IGRF-12 model (Fig.
422 5l). Since 1900, the S-RFP is divided into two different RFPs: one located in Patagonia and the second
423 located under South Africa. Recent studies [Pavón-Carrasco & De Santis, 2016; Terra-Nova et al.,
424 2017] indicate that, nowadays, the Patagonian RFP is vanishing and the South African RFP is
425 reinforcing. Our new reconstruction does not have enough resolution to establish if the strong
426 westward movement of the S-RFP observed between 1700 and 1900 AD corresponds to a real
427 movement of a single or two close RFPs.
428 It is considered that RFPs are formed by upwelling structures of the toroidal field on the
429 outer core boundary [Gubbins & Bloxham, 1986; Wicht & Olson, 2004; Takahashi et al., 2007; Amit
430 & Christensen, 2008; Aubert et al., 2008; Olson et al., 2009]. Tarduno et al. [2015] proposed that the
431 African large low shear velocity province located beneath South Africa controls the location of core
432 flux expulsions that ultimately control the location and origin of the SAA. Later, Terra-Nova et al.
433 [2016] explored the possibility that RFPs had preferred locations prescribed by lower mantle lateral
434 heterogeneity, which would suppose mantle control on RFPs positions. On paleomagnetic models
435 for the last 9000 years, they observed two longitudinal regions of higher RFPs concentration. The
436 first one located between longitudes 80◦W and 50◦E, and the second between 90◦E and 170◦E. The
437 S-RFP evolved between 62ºE to 32º W (Fig. 5), covering the first of the regions proposed by Terra-
438 Nova et al. [2016]. On average, during the 1500-1900 AD interval the preferred location of the S-
439 RFP was beneath South Africa.

In addition to the intense and persistent RFP related to the SAA (Fig. 4), other intriguing feature of the geomagnetic field is revealed by the SHAWQ2k model: a RFP located in the northern hemisphere (called N-RFP in Fig. 5). This N-RFP was also identified by Terra-Nova et al. [2015] around 1520 AD. Our study suggests that the emergence of the N-RFP occurred between 1000 and 1400 AD, when a "tongue" of reversed polarity penetrated from the magnetic equator towards the North Atlantic at a rate of 10.4 km/yr (a similar velocity that for S-RFP). The N-RFP drifted northeast and appeared clearly isolated around 1700 AD beneath the United Kingdom and the Scandinavian region, where it remained up to now. The intensity of the N-RFP has decreased 55% from 1550 to 1900 and is vanishing at present times (see Fig. 5). The intriguing antisymmetric evolution of the N-RFP related to the S-RFP should be investigated in more detail.

One of the earliest and most prominent observations of geomagnetism was the westward drift of field structures observed in historical times [e.g., Bullard et al., 1950; Yukutake, 1967; Bloxham & Gubbins, 1985; Finlay & Jackson, 2003]. Although the core flow is probably more complex, the zonal part of core flow models is often westward at low and middle latitudes, in particular, in the Southern Hemisphere [Amit & Olson, 2006]. Recently, it was argued that the westward drift is caused by the gravitational coupling between the inner core and the mantle [Aubert, 2013; Aubert et al., 2013]. However, the dynamical origin of the westward drift is still under debate. Dumberry & Finlay [2007] and Wardinsky & Korte [2008] studied the geomagnetic flux motions at the CMB using the CALS7k.2 model. They observed that eastward and westward azimuthal motions occur alternatively for the last 7 ka. Here, we find that S-RFPs exhibited a clear southern and westward drift, while the N-RFP drifted northeast. This new finding still awaits an explanation but suggests that thermal core–mantle interactions influence the geometry of the observed field motions at the CMB as proposed by Dumberry & Finlay [2007].

In order to evaluate the non-dipole contributions to the RFPs we have also calculated the Br at the CMB for $n = 1$ (dipole), $n = 2$ (adding quadrupole), $n = 3$ (adding octupole) and $n = 6$ (maximum degree used at the CMB). In Fig. 6, we show the results obtained for 1700 AD, when the S-RFP is isolated. We can clearly observe that both N and S lobes are mainly due to harmonic degrees greater than 3. Quadrupole and octupole contributions are important because they break the symmetry of

468 the dipole beneath South Africa, where the S-RFP is isolated. The N-RFP is exclusively due to non-
469 dipole terms of higher degree.

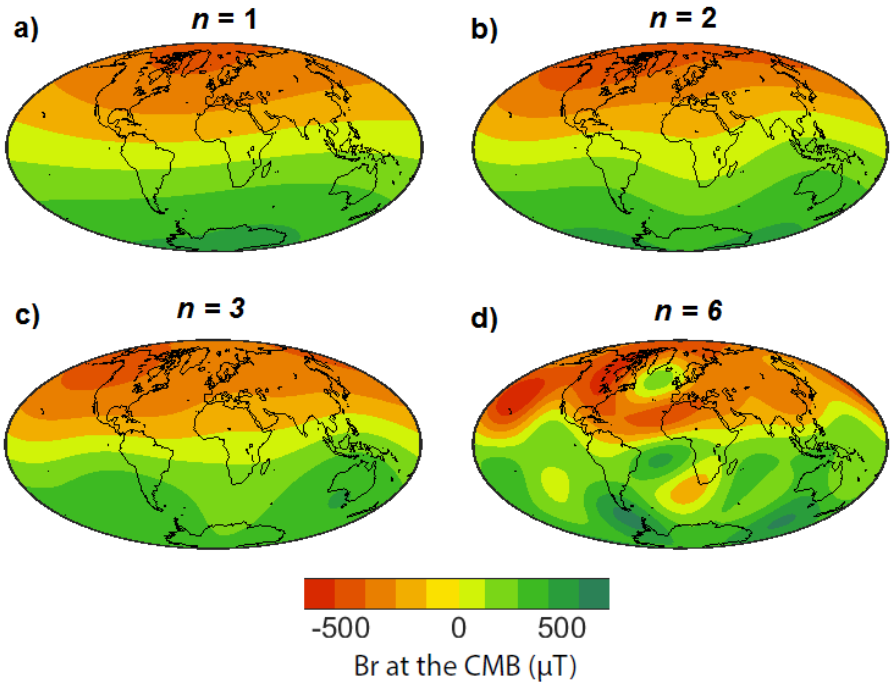

470

471 **Fig. 6. Harmonic contributions of the Br at the CMB.** Different spherical harmonics
472 contributions of the Br component at the CMB in 1700 AD, when the S-RFP isolated.

473

474 ## 5. Conclusions

475 The new paleomagnetic data, especially those coming from Africa and South America, and
476 the imposition of a weighing quality scheme during the modeling process have allowed us to obtain
477 an improved reconstruction of the evolution of past geomagnetic field over the last 2 ka with
478 unprecedented resolution.

479 Regarding the evolution of the SAA, interesting outcomes have been found. The RFP
480 observed at the CMB associated with the SAA seems to emerge in the Southern Hemisphere from at
481 least 950 AD. In addition, another RFP has been identified in the North Atlantic region. Both RFPs
482 evolved from equatorial regions towards higher latitudes. Understanding the physical mechanism
483 responsible for their temporal evolution is a crucial point to better understand the dynamic of the
484 geomagnetic field. Are these RFPs due to random core motions or a reflection of structure at the
485 CMB? In order to shed light on this question, new high quality archeomagnetic data are still necessary

to further define the past behaviour of the RPFs, especially from the Southern Hemisphere. It is also important to highlight that the use of an appropriated weighting scheme based on data accuracy seems to improve our understanding of the past geomagnetic field.

Acknowledgements

Authors are grateful to the research projects CGL2014-54112-R, CGL2015-63888-R, CGL2017-87015-P and CGL2017-92285-EXP of the Spanish Ministerio de Economía y Competitividad. SAC thanks the FPI grant BES-2012-052991, which allowed developing this work. MGP also acknowledges the Ramón y Cajal Program of the Spanish Ministerio de Economía y Competitividad and the PICS International Program for Scientific Cooperation (CNRS-France and CSIC-Spain). Authors are very grateful to one anonymous reviewer for his/her careful and detailed review, which has helped to improve the quality of the manuscript substantially. The AV database is presented in the Table 5S of the Supplementary Material, which specifies if a paleomagnetic datum has been considered of quality (named as "Q" in the last column of this table).

References

Amit, H., and Christensen, U. (2008) Accounting for magnetic diffusion in core flow inversions from geomagnetic secular variation. *Geophys. J. Int.* 175: 913–924.

Aubert, J. (2013) Flow throughout the Earth's core inverted from geomagnetic observations and numerical dynamo models. *Geophys. J. Int.* 192(2): 537-556.

Aubert, J. (2015) Geomagnetic forecasts driven by thermal wind dynamics in Earth's core. *Geophys. J.Int.* 203:1738–1751, doi:10.1093/gji/ggv394.

Aubert, J., Amit, H., Hulot, G., and Olson, P. (2008) Thermo-chemical flows couple the Earth's inner core growth to mantle heterogeneity. *Nature* 454: 758–761.

Aubert, J., Finlay, C.C., Fournier, A. (2013) Bottom-up control of geomagnetic secular variation by the Earth's inner core. *Nature* 502: 219-223.

Bloxham, J., and Gubbins, D. (1985) The secular variation of the Earth's magnetic field. *Nature* 317: 777-781.

514 Brown, M.C., Donadini, F., Korte, M., Nilsson, A., Korhonen, K., Lodge, A., Lengyel, S.N.,
515 Constable, C.G. (2015) GEOMAGIA50.v3: 1. General structure and modifications to the
516 archeological and volcanic database. *Earth Planets Space* 67:83, doi: 10.1186/s40623-015-0232-0.
517 Bullard, E. C., Freedman, C., Gellman, H., Nixon, J. (1950) The westward drift of the Earth's
518 magnetic field. *Philos. Trans. R. Soc. London Ser. A.* 243, 67.
519 Burlatskaya, S. P., Nachasova, I. E., Didenko, E. J., Shelestun, N. K. (1986), Archeomagnetic
520 Determinations of Geomagnetic Field Elements, *Sov. Geophys. Comm. of the USRR Acad. of Sci.*,
521 Moscow.
522 Chauvin, A., Y. Garcia, P. Lanos, and F. Laubenheimer (2000) Paleointensity of the geomagnetic
523 field recovered on archaeomagnetic sites from France. *Phys. Earth Planet. Inter.* 120: 111–136.
524 Constable, C., Korte, M., Panovska, S. (2016) Persistent high paleosecular variation activity in
525 southern hemisphere for at least 10000 years. *Earth Planet. Sci. Lett.* 453: 78–86.
526 Cromwell, G., Tauxe, L., Staudigel, H., & Ron, H. (2015) Paleointensity estimates from historic and
527 modern Hawaiian lava flows using glassy basalt as a primary source material. *Phys. Earth Planet.*
528 *Inter.* 241: 44-56.
529 De Boor, C. (2001) A Practical Guide to Splines (Springer, New York).
530 De Santis, A., Qamili, E., Wu, L. (2013) Toward a possible next geomagnetic transition? *Nat. Hazards*
531 *Earth Syst. Sci.* 13: 3395–3403, doi: 10.5194/nhess-13-3395-2013.
532 Donadini, F., Serneels, V., Kapper, L., El Kateb, A. (2015) Directional changes of the geomagnetic
533 field in West Africa: Insights from the metallurgical site of Korsimoro. *Earth Planet. Sci. Lett.*, 430:
534 349–355.
535 Dumberry, M. and Finlay, C.C. (2007) Eastward and westward drift of the Earth's magnetic field for
536 the last three millennia. *Earth Planet. Sci. Lett.* 254: 146–157.
537 Eighmy, J. (2003) Archeomagnetic laboratory results for the Inca, Spanish and Indigenous silver
538 production Project Porco. *Bolivia. Laboratory Report*, Colorado State University, Fort Collins, CO.
539 11.
540 Finlay, C., and Jackson, A. (2003) Equatorially dominated magnetic field change at the surface of
541 earth's core. *Science* 300: 2084–2086.

542 Finlay, C.C., Aubert, J., Gillet, N. (2016) Gyre-driven decay of the Earth's magnetic dipole. *Nat.*
543 *Commun.* 7:10422, doi:10.1038/ncomms10422.
544 Genevey, A., Gallet, Y., Constable, C., Korte, M., Hulot, G. (2008) ArcheoInt: An upgraded
545 compilation of geomagnetic field intensity data for the past ten millennia and its application to
546 the recovery of the past dipole moment. *Geochem. Geophys. Geosyst.* 9 (4), Q04038.
547 Genevey, A., Gallet, Y., Margueron, J. (2003) Eight thousand years of geomagnetic field intensity
548 variations in the eastern Mediterranean. *J. Geophys. Res.* 108(B5), 2228, doi:10.1029/2001JB001612.
549 Goguitchaichvili, A., D. Loponte, J. Morales, A. Acosta (2012) The Archaeointensity of the Earth's
550 Magnetic Field retrieved from Pampean Ceramics (South America). *Archaeometry* 54 (2): 388–400.
551 Goguitchaichvili, A., J. Morales, D. Schavelzon, C. Vásquez, C.S.G. Gogorza, D. Loponte, A.
552 Rapalini (2015) Variation of the Earth's magnetic field strength in South America during the last
553 two millennia: New results from historical buildings of Buenos Aires and re-evaluation of regional
554 data. *Phys. Earth Planet. Inter.* 245: 15–25.
555 Gubbins, D., and Bloxham, J. (1985) Geomagnetic field analysis. III. Magnetic fields on the core–
556 mantle boundary. *Geophys. J. R. Astron. Soc.* 80: 695–713.
557 Gubbins, D., Jones, A. L., Finlay, C. C. (2006) Fall in Earth's magnetic field is erratic. *Science*
558 312(5775): 900–902.
559 Hollerbach, R., and Gubbins, D. (2007) Inner Core Tangent Cylinder. *Encyclopedia of Geomagnetism*
560 *And Paleomagnetism*, Springer (The Netherlands).
561 Hulot, G., Eymin, C., Langlais, B., Mandea, M., Olsen, N. (2002) Small-scale structure of the
562 geodynamo inferred from Ørsted and Magsat satellite data. *Nature* 416: 620–623.
563 Jackson, A., Jonkers, A.R.T., Walker, M.R. (2000) Four centuries of geomagnetic secular variation
564 from historical records. *Philos. Trans. R. Soc. Lond. A.* 358 (1768): 957-990.
565 Kapper, L., Donadini, F., Serneels, V., Tema, E., Goguitchaichvili, A., Morales, J.J. (2017)
566 Reconstructing the Geomagnetic Field in West Africa: First Absolute Intensity Results from
567 Burkina Faso. *Scientific Reports*, 7, doi: 10.1038/srep45225.
568 Korte, M., and Constable, C.G. (2005) Continuous geomagnetic field models for the past 7 millennia:
569 2 CALS7K. *Geochem. Geophys. Geosyst.* 6, Q02H16.

570 Korte, M., and Constable, C.G. (2008) Spatial and temporal resolution of millennial scale geomagnetic
571 field models. *Adv. Space Res.* 41: 57–69. http://dx.doi.org/10.1016/j.asr.2007.03.094.
572 Korte, M., and Constable, C.G. (2011) Improving geomagnetic field reconstructions for 0-3 ka. *Phys.*
573 *Earth Planet. In.* 188: 247-259.
574 Korte, M., and Holme, R. (2010) On the persistence of geomagnetic flux lobes in global Holocene
575 field models. *Phys. Earth Planet. Inter.* 182: 179-186.
576 Korte, M., and Mandea, M. (2008) Magnetic poles and dipole tilt variation over the past decades to
577 millennia. *Earth Planets Space*. 60 (9): 937-948.
578 Korte, M., Donadini, C., Constable, C.G. (2009) The geomagnetic field for 0-3 ka, part II: a new
579 series of time-varying global models. *Geochem. Geophys. Geosyst.* 10, Q06008.
580 Laj, C., and Kissel, C. (2015) An impending geomagnetic transition? Hints from the past. *Front. Earth*
581 *Sci.* 3:61, doi:10.3389/feart.2015.00061.
582 Licht, A., Hulot G., Gallet Y., Thébault E. (2013) Ensembles of low degree archeomagnetic field
583 models for the past three millennia. *Phys. Earth Planet. Inter.* 224: 38-67.
584 Mitra, R., Tauxe, L., McIntosh, S.K. (2013) Two thousand years of archeointensity from West Africa.
585 *Earth Planet. Sci. Lett.* 364: 123–133. http://dx.doi.org/10.1016/j.epsl.2012.12.027.
586 Néel, L. (1955) Some theoretical aspects of rock. *Adv. Phys.* 4: 191–243.
587 Neukirch, L. P., Tarduno, J. A., Huffman, T. N., Watkeys, M. K., Scribner, C. A., Cottrell, R. D.
588 (2012) An archeomagnetic analysis of burnt grain bin floors from ca. 1200 to 1250 AD Iron-Age
589 South Africa. *Phys. Earth Planet. Inter.* 190–191: 71–79, doi:10.1016/j.pepi.2011.11.004.
590 Nilsson, A., Holme, R., Korte, M., Suttie, N., Hill, M. (2014) Reconstructing Holocene geomagnetic
591 field variation: new methods, models and implications. *Geophys. J. Int.* 198(1): 229–248.
592 Nilsson, A., Muscheler, R., Snowball, I. (2011) Millennial scale cyclicity in the geodynamo inferred
593 from a dipole tilt reconstruction. *Earth Planet. Sci. Lett.* 311: 299–305.
594 Nilsson, A., Snowball, I., Muscheler, R., Uvo, C. B. (2010) Holocene geocentric dipole tilt model
595 constrained by sedimentary paleomagnetic data. *Geochem. Geophys. Geosyst.* 11, Q08018,
596 doi:10.1029/2010GC003118.

597 Noël, M., and Batt, C.M. (1990) A method for correcting geographically separated remanence
598 directions for the purpose of archaeomagnetic dating. *Geophys. J. Int.* 102: 753 – 756.
599 Olson, P., and Amit, H. (2006) Changes in Earth's dipole. *Naturwissenschaften* 93: 519–542.
600 Olson, P., Driscoll, P., and Amit, H. (2009) Dipole collapse and reversal precursors in a numerical
601 dynamo. *Phys. Earth. Planet. Inter.* 173: 121–140.
602 Osete, M.L., Catanzariti, G., Chauvin, A., Pavón-Carrasco, F.J., Roperch, P., Fernández, V.M. (2015)
603 First archaeomagnetic field intensity data from Ethiopia, Africa (1615 ± 12 AD). *Phys. Earth Planet.*
604 *In.* 242: 24–35.
605 Paterson, G.A., Tauxe, L., Biggin, A.J., Shaar, R., Jonestrask, L.C. (2014) On improving the selection
606 of Thellier-type paleointensity data. *Geochem. Geophys. Geosyst.* 15: 1180–1192.
607 http://dx.doi.org/10.1002/2013GC005135.
608 Pavón-Carrasco, F.J., and De Santis, A. (2016) The South Atlantic Anomaly: The Key for a Possible
609 Geomagnetic Reversal. *Front. Earth Sci.* 4:40, doi: 10.3389/feart.2016.00040.
610 Pavón-Carrasco, F.J., Osete, M.L., Torta, J.M., De Santis, A. (2014a) A geomagnetic field model for
611 the Holocene based on archaeomagnetic and lava flow data. *Earth Planet. Sci. Lett.* 388: 98-109.
612 Pavón-Carrasco, F. J., Gómez-Paccard, M., Hervé, G., Osete, M. L., Chauvin, A. (2014b) Intensity
613 of the geomagnetic field in Europe for the last 3ka: influence of data quality on geomagnetic field
614 modeling. *Geochem. Geophys. Geosyst.* 15, doi: 10.1002/2014GC005311.
615 Poletti, W., Trindade, R.I.F., Hartmann, G.A., Damiani, N., Rech, R.M. (2016) Archeomagnetism of
616 Jesuit Missions in South Brazil (1657–1706 AD) and assessment of the South American database.
617 *Earth Planet. Sci. Lett.* 445: 36–47.
618 Roberts, A.P., Tauxe, L., Heslop, D. (2013) Magnetic paleointensity stratigraphy and high-resolution
619 Quaternary geochronology: successes and future challenges. *Quaternary Sci. Rev.* 61: 1-16.
620 Roperch, P., Chauvin, A., Lara, L.E., Moreno, H. (2015) Secular variation of the Earth's magnetic
621 field and application to paleomagnetic dating of historical lava flows in Chile. *Phys. Earth Planet.*
622 *Inter.* 242: 65–78.

623 Roperch, P., Chauvin, A., Le Pennec, J.L., Lara, L.E. (2014) Paleomagnetic study of juvenile basaltic-
624 andesite clasts from Andean pyroclastic density current deposits. *Phys. Earth Planet. Inter.* 227: 20–
625 29.
626 Shah, J., Koppers, A.A.P., Leitner, M., Leonhardt, R., Muxworthy, A.R., Heunemann, C., Bachtadse,
627 V., Ashley, J.A.D, Matzka, J. (2016) Palaeomagnetic evidence for the persistence or recurrence of
628 geomagnetic main field anomalies in the South Atlantic. *Earth Planet Sci. Lett.* 441: 113–124.
629 Suttie, N., Holme, R., Hill, M. J., Shaw, J. (2011) Consistent treatment of errors in archaeointensity
630 implies rapid decay of the dipole prior to 1840. *Earth Planet Sci. Lett.* 304: 13–21.
631 Takahashi, F., Matsushima, M., Honkura, Y. (2007) A numerical study on magnetic polarity transition
632 in an MHD dynamo model. *Earth Planets Space* 59: 665–673.
633 Tarduno, J.A. (1990) Absolute Inclination Values from Deep Sea Sediments: A Reexamination of the
634 Cretaceous Pacific Record. *Geophys. Res. Lett.* 17: 101-104.
635 Tarduno, J.A., Tian, W., Wilkison, S. (1998) Biogeochemical remanent magnetization in pelagic
636 sediments of the western equatorial Pacific Ocean. *Geophys. Res. Lett.* 25: 3987-3990.
637 Tarduno, J.A., Watkeys, M.K., Huffman, T.N., Cottrell, R.D., Blackman, E.G., Wendt, A., Scribner,
638 C.A., Wagner, C.L. (2015) Antiquity of the South Atlantic Anomaly and evidence for top-down
639 control on the geodynamo. *Nat. Commun.* 6, doi: 10.1038/ncomms8865.
640 Tauxe, L. (1993) Sedimentary records of relative paleointensity: theory and practise. *Rev. Geophys.* 31:
641 319-354.
642 Terra-Nova, F., Amit, H., Hartmann, G.A., Trindade, R.I.F. (2015) The time-dependence of reversed
643 archaeomagnetic flux patches. *J. Geophys. Res.* 120 (2): 691–704.
644 Terra-Nova, F., Amit, H., Hartmann, G.A., Trindade, R.I.F. (2016) Using archaeomagnetic field
645 models to constrain the physics of the core: robustness and preferred locations of reversed flux
646 patches, *Geophys. J. Int.* 206 (3): 1890–1913. http://dx.doi.org/10.1093/gji/ggw248.
647 Terra-Nova, F., H. Amit, G. A. Hartmann, R.I.F. Trindade, K.J. Pinheiro (2017) Relating the South
648 Atlantic Anomaly and geomagnetic flux patches. *Phys. Earth Planet. Inter.* 266: 39-53.
649 Thébault, E., et al. (2015) International Geomagnetic Reference Field: the 12th generation. *Earth*
650 *Planets Space* 67:79, doi: 10.1186/s40623-015-0228-9.

651 Thellier, E., and O. Thellier (1959) Sur l'intensité du champ magnétique terrestre dans le passé
652 historique et géologique. *Ann. Geophys.* 15: 285–376.
653 Wardinski, I. and Korte, M. (2008) The evolution of the core-surface flow over the last seven
654 thousands years. *J. Geophys. Res.* 113, B05101, doi:10.1029/2007JB005024.
655 Wicht, J., and Olson, P. (2004) A detailed study of the polarity reversal mechanism in a numerical
656 dynamo model. *Geochem. Geophys. Geosyst.* 5(3): Q03H10, doi:10.1029/2003GC000602.
657 Yukutake, T. (1967) The westward drift of the Earth's magnetic field in historic times. *J. Geomagn.*
658 *Geoelectr.* 19(2).